

Electromagnetic signals from Au+Au collisions at RHIC energy $\sqrt{s_{NN}}=200$ GeV and Pb+Pb collisions at LHC energy, $\sqrt{s_{NN}}=2.76$ TeV.

Jajati K. Nayak and Bikash Sinha

Variable Energy Cyclotron Centre, 1/AF, Bidhan Nagar, Kolkata - 700064

(Dated: February 21, 2022)

We analyse the recently available experimental data on direct photon productions from Au+Au collisions at $\sqrt{s_{NN}}=200$ GeV RHIC and from Pb+Pb collisions at $\sqrt{s_{NN}}=2.76$ TeV LHC energies. The transverse momentum (p_T) distributions have been evaluated with the assumption of an initial quark gluon plasma phase at temperatures $T_i=404$ and 546 MeV with initial thermalisation times $\tau_i=0.2$ and 0.1 fm/c respectively for RHIC and LHC energies. The theoretical evaluations agree reasonably well with the experimental observations. The thermal window for the LHC energy is justified through the ratio of the p_T spectra of thermal photons to dileptons.

PACS numbers: 25.75.-q, 25.75.Dw, 24.85.+p

It is by now conventional wisdom, that collisions between two nuclei at RHIC as well as LHC energies will lead to the formation of quark gluon plasma (QGP). Although the exact nature of QGP-hadron phase transition is still plagued by uncertainties, but there are several evidences that QGP is formed [1–4] at RHIC energies. It has long been recognised that promising signals of QGP are photons and dileptons [5–9]. The very nature of electromagnetic interactions ensures that the thermometric signals ($\gamma, \mu^+\mu^-, e^+e^-$) escape the QGP medium without any significant interaction, thus retaining the pristine information of QGP immediately after its formation. It has been pointed out by one of the authors and his collaborators, consistently for a long time [8–14], that the photons emanating from thermal medium show up in the p_T window of $1.5 \leq p_T(\text{GeV}) \leq 3.5$. It has also been pointed out [15, 16] during the early days of QGP physics and now, that the ratio $\gamma/\mu^+\mu^-$ eliminates some of the uncertainties associated with the input parameters used in the model.

The concept of ratio has been revisited again in ref [17, 18] where the sensitivities of the of the initial parameters have been studied extensively. The formation of a thermal medium is manifested by the flattening of the ratio beyond certain p_T . Now that the direct photon data has come out of LHC we tend to analyse the data and test the above prediction at $\sqrt{s_{NN}}=2.76$ TeV.

It is quite remarkable that the original theoretical prediction [15–18] turns out to be valid also at LHC energies with added advantage that the very high energy of LHC turns the invariant mass M , of dileptons less relevant compare to (say) at RHIC energies.

It should also be noted that there is already a tantalising hint of QGP formation even at SPS energy [19, 20]. In the following work we present our

findings of this interesting phenomenon. Thus over a wide range of energies going through orders of magnitude, it is quite exciting to note that p_T window for thermal photons and dileptons remains the same as predicted earlier, only the range of window increases almost upto 4 GeV or more at LHC energy.

In this present work we have evaluated the direct photon productions from (i) Au+Au collisions at $\sqrt{s_{NN}}=200$ GeV for 0-5% centrality and (ii) Pb+Pb collisions at $\sqrt{s_{NN}}=2.76$ TeV for 0-40% centrality and finally compared with the recently available data [21] for RHIC and [24] for LHC energies. We analyse the data using our earlier approach, which has been used consistently to explain the SPS [14] and RHIC [13] data for different centralities. The invariant thermal yield of photons is evaluated from the production rate as in ref [17, 25] and using the (2+1) dimensional relativistic hydrodynamics. The photon contributions from prompt productions have been evaluated using the parton distribution function as parametrised in *Cteq6M*. Different thermal sources of photon productions are considered as in ref [17, 25] and sources of prompt productions as in ref [10, 26]. The authors in [27] also mention the contribution of jet-plasma interaction to the high p_T photons. Here the data seems to be explained nicely without considering the above phenomenon. The dilepton productions are evaluated as in [20] using the equation of state mentioned in sec-II. Then we evaluate ratio of the transverse momentum spectra of thermal photons to dileptons to seek out the thermal window at $\sqrt{s_{NN}}=2.76$ TeV.

In section II the prompt and thermal photon productions have been discussed. In the following section the expansion dynamics of the produced system, along with the initial conditions, is described. Finally, the results have been discussed and compared with the available data. The summary is presented last.

On the basis of sources of production, photons emanating from the relativistic heavy ion collision, can be broadly categorized as follows; (i) prompt photons resulting from the interactions of the partons of the colliding nuclei, (ii) pre-equilibrium photons, emitted before the medium gets thermalised, (iii) thermal photons originating from the interaction of thermal partons as well as thermal hadrons, (iv) photons produced from the passage of jets through plasma and (v) the photons from the decay of long lived hadrons ($\pi^0 \rightarrow \gamma\gamma$, $\eta \rightarrow \gamma\gamma$, etc). The aim of this work is to analyse the photon data from RHIC and LHC energies, where photons from the hadronic decays, have already been excluded. Out of the remaining categories, the pre-equilibrium contributions is negligible since thermalisation times (τ_i) for RHIC and LHC are very small. The photons due to the passage of jets through the medium is not considered here. In this work, we consider the prompt and thermal photons-the two main sources of direct photons, in terms of their transverse momentum (p_T) distribution.

The prompt photons originate from the initial hard scatterings of the partons, primarily because of the compton processes ($q(\bar{q}) + g \rightarrow q(\bar{q}) + \gamma$), annihilation process ($q + \bar{q} \rightarrow g + \gamma$) and quark fragmentation ($q(\bar{q}) \rightarrow q(\bar{q}) + \gamma$) following the scattering of partons of the nucleus in the colliding nuclei. In a complete and consistent NLOpQCD [$O(\alpha_s^2)$] calculation, it is important to account for the prompt photons arising from various $2 \rightarrow 3$ processes [28, 29]. This calculation is comparable with the leading order calculation [10] with a higher K factor. We use this calculation and scale it up by the number of binary collisions for Au+Au and Pb+Pb collisions at $\sqrt{s_{NN}}=200$ GeV (RHIC) and 2.76 TeV (LHC) energies respectively. The intrinsic k_T smearing is ignored here.

The p_T distribution of thermal photons is expressed in terms of invariant yield as follows;

$$\frac{d^2 N_\gamma}{d^2 p_T dy} = \sum_{i=\text{phases}} \int_i \left(\frac{d^2 R_\gamma}{d^2 p_T dy} \right)_i d^4 x \quad (1)$$

N_γ is the number of photons produced. y is the rapidity. where i represents QGP and Hadronic phases. $\left(\frac{d^2 R_\gamma}{d^2 p_T dy} \right)_i$ is the static rate of photon production at a temperature T from phase i . $d^4 x$ is the four volume element and its evolution is taken care by relativistic ideal hydrodynamics. The photon emission rate is given as follows;

$$\frac{d^2 R}{d^2 p_T dy} = \frac{g^{\mu\nu}}{(2\pi)^3} \text{Im} \Pi_{\mu\nu} f_{BE} \quad (2)$$

(see [5–9] for details). $\text{Im} \Pi_{\mu\nu}$ is the imaginary part of the retarded photon self energy. f_{BE} is the thermal distribution function. ($g^{\mu\nu} = -\sum_{\text{polarization}} \epsilon^\mu \epsilon^\nu$).

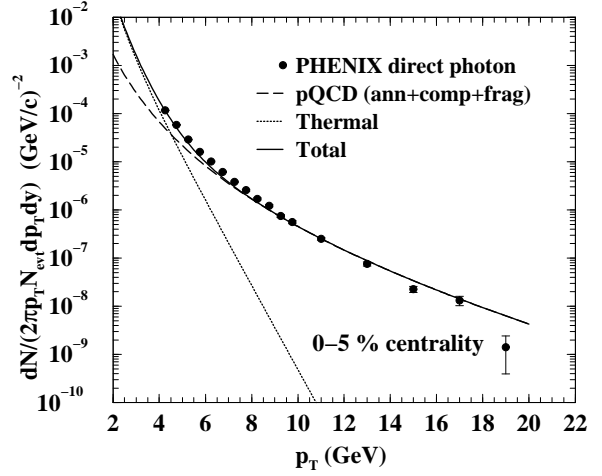


FIG. 1: The p_T spectra of direct photons from Au+Au collisions at $\sqrt{s_{NN}}=200$ GeV RHIC energy from different sources.

The static emission rate of photons for QGP and hadronic phases are calculated from various partonic and hadronic processes.

The photon emission rate from QGP due to compton ($q(\bar{q})g \rightarrow q(\bar{q})\gamma$) and annihilation ($q\bar{q} \rightarrow g\gamma$) processes were evaluated [30, 31] by using hard thermal loop (HTL) approximation [32]. Further it was found [33] that photon productions from the reactions, $gq \rightarrow gq\gamma$, $qq \rightarrow qq\gamma$, $qq\bar{q} \rightarrow q\gamma$ and $gq\bar{q} \rightarrow g\gamma$ contribute in the same order as annihilation and compton processes do. The suppression due to multiple scattering during the emission process which was not mentioned in [30, 31, 33] was later discussed in Ref. [34]. The complete calculation of photon emission rate from QGP to order $O(\alpha_s)$ has been completed by resumming ladder diagrams in the effective theory [35], which has been used in the present work. The emission rates for various processes are available in parametrised form in Ref. [36]. Here we use the temperature dependence of the strong coupling constant from Ref. [37].

An exhaustive set of hadronic interactions have been considered to evaluate the photon emission rate from a hadronic phase. The relevant processes are basically; (i) $\pi\pi \rightarrow \rho\gamma$, (ii) $\pi\rho \rightarrow \pi\gamma$ (with π , ρ , ω , ϕ and a_1 in the intermediate state [38]), (iii) $\pi\pi \rightarrow \eta\gamma$ and (iv) $\pi\eta \rightarrow \pi\gamma$. Also the radiative decay of higher resonance states [38–41] such as, $\rho \rightarrow \pi\pi\gamma$ and $\omega \rightarrow \pi\gamma$ produces photons. The corresponding vertices can be obtained from various phenomenological Lagrangians as described in detail in Ref. [38–41]. The contributions from the reactions involving strange mesons like $\pi K^* \rightarrow K\gamma$, $\pi K \rightarrow K^*\gamma$, $\rho K \rightarrow K\gamma$ and $KK^* \rightarrow K\gamma$, have been pointed out in [42] Contributions from other decays,

such as $K^*(892) \rightarrow K\gamma$, $\phi \rightarrow \eta\gamma$, $b_1(1235) \rightarrow \pi\gamma$, $a_2(1320) \rightarrow \pi\gamma$ and $K_1(1270) \rightarrow \pi\gamma$ have been found to be small [43] for $p_T > 1$ GeV. We consider all the processes for our calculation. All the isospin combinations for the above reactions and decays have properly been taken into account. The effects of hadronic form factors(dipole) [42] have been incorporated.

When two energetic heavy nuclei collide with each other, a large amount of energy and thus entropy is channeled into a small volume. The produced system achieve thermalisation in a short time because of the secondary interactions and the matter then expands due to the high internal pressure. The space-time evolution of the matter has been studied using ideal relativistic hydrodynamics [44] with longitudinal boost invariance [45] and cylindrical symmetry. In the present analysis of Pb+Pb collisions we consider the initial energy density ($\epsilon(\tau_i, r)$) and radial velocity ($v(\tau_i, r)$) profiles similar to our earlier studies [14, 17, 20, 25]. Transition temperature which is an input parameter to the hydrodynamic calculation is taken as $T_c=163$ MeV according the recent works of lattice QCD computation by the HotQCD Collaboration [46] and by the Bielefield Group [47]. We also consider $T_c=170$ MeV as predicted by the lattice computation from other group [48] to compare the results. The initial temperature T_i and initial thermalisation time τ_i are constrained from the following equation [49];

$$T_i^3(b) \equiv \frac{2\pi^4}{45\zeta(3)} \frac{1}{\pi R^2 \tau_i} \frac{90}{4\pi^2 g_{eff}} \frac{dN}{dy}(b), \quad (3)$$

where $\zeta(3)$ denotes the Riemann zeta function, R is the radius [$\sim 1.1(N_{part}/2)^{1/3}$, N_{part} is the number of participant nucleons] of the colliding system, τ_i is the initial thermalisation time and g_{eff} is the statistical degeneracy taken to be 37, considering a 2-flavor QGP to be produced initially. $dN/dy(b)$ is the hadron (mostly pion) multiplicity for a given impact parameter b , which is obtained from the Glauber model for 0-40% collision centrality of Pb+Pb collisions at $\sqrt{s_{NN}}=2.76$ TeV. The initial temperature obtained from the above equation Eq.3 for $dN/dy(b)=1275$ and $\tau_i=0.1$ fm is 546 MeV.

The heavy ion collision experiment at LHC energy maps the region, where the value of baryonic chemical potential, μ_B is small and the temperature is rather high. Guided by the lattice computation, which predicts a crossover from hadronic to partonic phase for $\mu_B=0$, we construct an equation of state (EOS) for the evolution dynamics which gives crossover like transition. We consider the entropy (s_q) of the QGP phase (for $T > T_c$) using BAG model EOS and the entropy (s_h) of the hadron gas (considering non-interacting hadrons and their res-

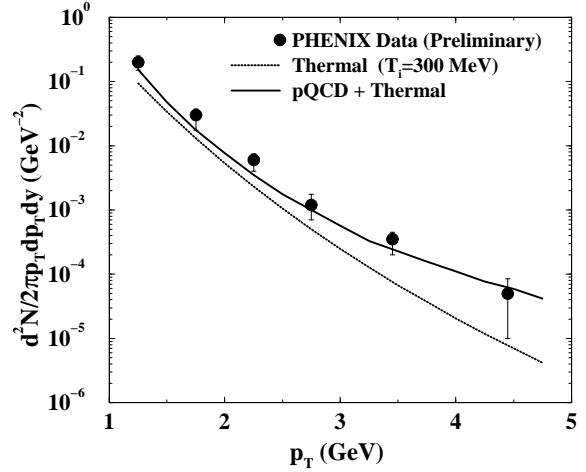


FIG. 2: Direct photons measured by PHENIX collaboration for 0-20% centrality at $\sqrt{s_{NN}}=200$ GeV [13].

onances up to mass ~ 2.5 GeV for $T < T_c$). The entropy during the transition region is parametrised using a tan-hyperbolic function [50] as follows.

$$s(T) = s_q(T)f_q(T) + [1 - f_q(T)]s_h(T) \\ \text{and } f_q(T) = \frac{1}{2}(1 + \tanh \frac{T - T_c}{\Gamma}) \quad (4)$$

Here Γ is the width parameter and assumes a finite value for crossover transition. This value can be tuned to zero to the first order transition. Here the width parameter is taken to be $\Gamma=20$ MeV. EOS which is an input to the hydrodynamic calculation has been constructed for a transition temperature $T_c=163$ MeV and width parameter $\Gamma=20$ MeV. The effective degeneracy $g(T)$ of the system which is obtained from the entropy $s(T)$ (Eq. 4).

The p_T spectra of direct photons have been evaluated for Au+Au collisions at $\sqrt{s_{NN}}=200$ GeV RHIC energy. For 0-5% of the centrality of the collision, the total pion multiplicity is taken as $dN/dy=1100$. To evaluate the thermal contribution, we consider an initial temperature $T_i=404$ MeV, which is obtained from the Eq. 3 for an initial thermalisation time $\tau_i=0.2$ fm. An equal time freeze out scenario for all the hadrons is assumed and the value of freeze out temperature T_f is taken to be 120 MeV, which is contrasted from the pion and kaon spectra [13]. The prompt photon contributions have been evaluated from the annihilation, compton and quark-fragmentation processes using pQCD calculations [10]. The calculation is done for $N_{coll}=910$ (obtain from Glauber model calculation for 0-5% centrality) and $\sigma_{in}=42$ mb. We use the parametrised parton distribution function from *Cteq6M*. To account for the next-to-next leading order contribution, the value of K_γ and K_{brem} is taken to be 1.4

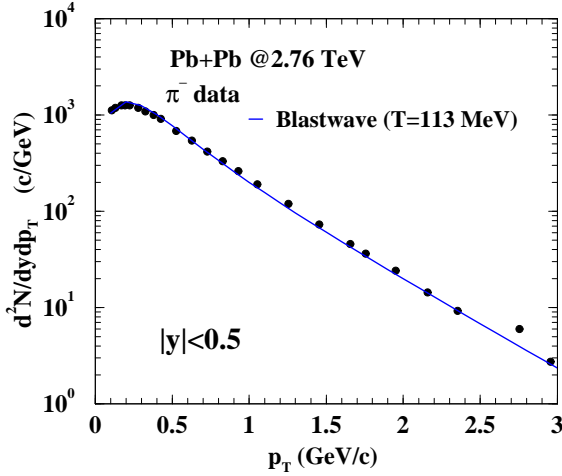


FIG. 3: The pion spectra from Pb+Pb collisions at $\sqrt{s_{NN}}=2.76$ TeV LHC energy fitted with blast wave with temperature $T_f=113$ MeV and $\beta=0.9$

and 2.2 respectively for RHIC energy. The results are shown in Fig. 1. The solid circles represent the recently published direct photon data from Au+Au collisions (0-5% centrality) by PHENIX collaboration [21]. The long-dashed and dotted lines represents the pQCD and thermal contributions respectively. The solid is for the sum total of both. T_c is taken to be 163 MeV.

The Fig. 2 displays the direct photon productions for 0-20% centrality of Au+Au collisions at RHIC energy [22] as per our earlier evaluation [13]. The dotted line represents the thermal contribution for lattice EOS [23] with $T_i=300$ MeV and $\tau_i=0.5$ fm. The prompt photons are evaluated by scaling the NLO calculation of Gordon and Vogelssang's [26] prediction for p-p collisions with the number of collisions for Au+Au. The solid line represents the total photons.

While evaluating the p_T distributions for direct photons at LHC energy, same time freezeout scenario for all the hadrons is assumed with $T_f=113$ MeV, which is constrained by the pion data. Fig. 3 displays the blast wave explanation of the pion data from Pb+Pb collisions at $\sqrt{s_{NN}}=2.76$ TeV (For data see [51]) with $T=113$ MeV.

In Fig. 4 the direct photon data from Pb+Pb collisions for 0-40% centrality at $\sqrt{s_{NN}}=2.76$ TeV measured by ALICE collaboration (solid circles) [24] is shown. The dotted line represents the pQCD calculation of annihilation and compton processes (prompt) using *Cteq6m* for $N_{coll}=853$ (for 0-40%). The solid line with open circles show the contributions from quark-fragmentation to the prompt photons. The long-dashed line is the sum over all the hard processes. $K_\gamma=3.2$ for annihilation and comp-

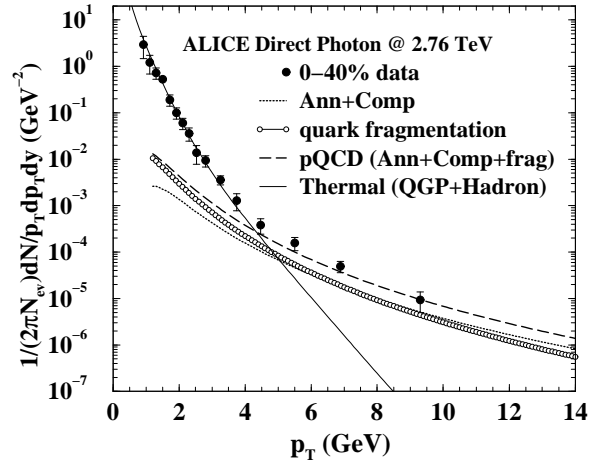


FIG. 4: The p_T spectra of direct photons from Pb+Pb collisions at $\sqrt{s_{NN}}=2.76$ TeV LHC energy from different sources.

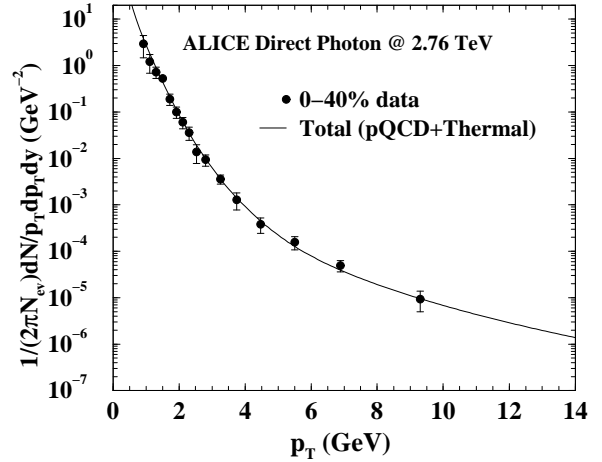


FIG. 5: The p_T spectra of direct photons from Pb+Pb collisions at $\sqrt{s_{NN}}=2.76$ TeV LHC energy. The solid circles are the data points measured by ALICE collaborations [21]. The solid line represents the theoretical evaluation.

ton processes and $K_{brem}=2.8$ for fragmentation process are considered to take the NNLO contributions into account. Considering T_i to be 546 MeV, which is obtained from Eq. 3 for 0-40% centrality and $\tau_i=0.1$ fm, $T_f=113$ MeV and $T_c=163$ MeV, the thermal contributions are evaluated from QGP and hadron gas. This is displayed in Fig. 4 (solidline). As depicted from Fig. 4, the thermal contribution dominates the invariant yield upto $p_T \sim 4$ GeV. The spectrum beyond $p_T > 4$ GeV is dominated by pQCD calculations clearly distinguishing thermal window $1.5 < p_T(\text{GeV}) < 4.0$. The solid line in Fig. 5 displays the sum of thermal and pQCD contributions

explaining the data within the ambit of considered parameters.

It is important to mention the sensitivity of the results due to the initial parameters. The transition temperature $T_c=163$ MeV is restricted from the results of lattice QCD computation by HotQCD and Bielefield group [46, 47]. However the computation as given in [48] predicts the value around ~ 170 MeV. To differentiate the effect of T_c we evaluate the photon spectra for LHC energy with $T_c=170$ MeV and found very little change in the p_T spectra. At $p_T=2$ GeV, the results for $T_c=170$ MeV is $\sim 1.2\%$ higher than $T_c=163$ MeV. The sensitivity of T_c is also found to be small in our earlier work [13]. The sensitivity of results to the initial temperature (in GeV) and thermalisation time (in fm) (T_i, τ_i) together is shown in Fig. 6. Comparing the multiplicity we consider ($T_i = 433, \tau_i = 0.2$) and reevaluate the photon spectra. The solid line is for ($T_i = 546, \tau_i = 0.1$) and the long-dashed line is for ($T_i = 0.433, \tau_i = 0.2$). At $p_T=2$ GeV the result differs by 7.54%. But the results are found to be sensitive to T_f . In Fig. 7 the prediction for direct photons at $\sqrt{s_{NN}}=5.5$ TeV is given with an initial QGP temperature $T_i=843$ MeV and $\tau_i=0.08$ fm. The charged particle multiplicity is taken to be 2500 for 0-5% centrality. It shows the dominance of thermal photons up to $p_T=4$ GeV of the direct photon spectra.

It has been argued since long [15, 16], that the ratio of the p_T spectra of thermal photons to lepton pairs forms a plateau in the p_T window $1.5 < p_T(\text{GeV}) < 3.5$ for different mass bins of lepton pairs and it is less sensitive to the input parameters. In ref [17] the ratio has been revisited and the sensitivities to different input parameters have been studied extensively. Here we study the ratio for $\sqrt{s_{NN}}=2.76$ TeV LHC energy for different mass window of the lepton pairs and plot the results in Fig. 8. The thermal dilepton yield is calculated using the approach mentioned in [20, 52], that explains the dimuon data from In+In collisions measured by NA60 collaboration. A plateau is observed beyond $p_T \sim 1.5$ GeV in Fig. 8.

The plateau in the ratio appears because of the following reason. The emission rate of photon and dilepton production show their momentum dependencies through their thermal phase space factor $f_{BE}(E, T)$ ($\sim \exp(-E/T)$). Where $E = M_T \cosh y$, $M_T = \sqrt{p_T^2 + M^2}$ & $y = \tanh^{-1} p_z/E$. p_z and y take their usual meanings. The nature of the spectra depends on M . When we consider the ratio of their momentum spectra at high p_T ($p_T \gg M$, & $M_T = p_T$), for a static system, then the real photon ($M^2 = 0$) and dilepton ($M^2 \neq 0$) have similar momentum dependence. Thus a plateau is observed in ratio for the static system. However for

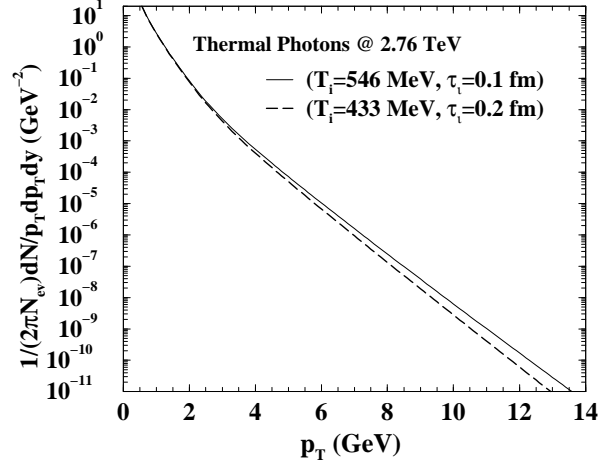


FIG. 6: Sensitivity in the production of thermal photons to T_i for LHC energy. The long dashed line represents the results for $T_i=433$ MeV and $\tau_i=0.2$ fm. Solid for $T_i=546$ MeV and $\tau_i=0.1$ fm

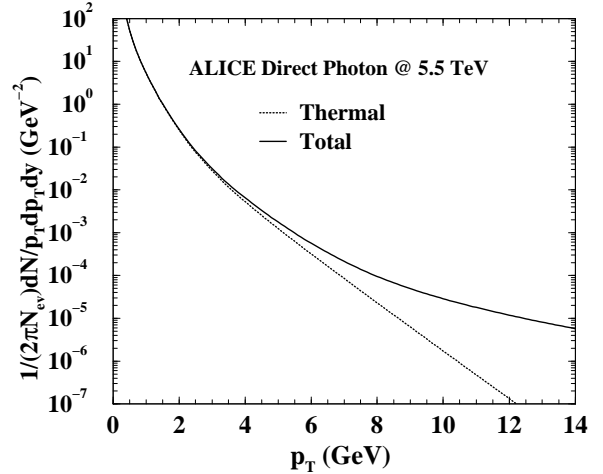


FIG. 7: Direct photon productions at $\sqrt{s_{NN}}=5.5$ TeV LHC energy.

a realistic case of an expanding system the thermal phase space factor goes as $f_{BE} \sim \exp(-u_\mu p^\mu)$, where u_μ and p_μ are the 4-velocity and -momentum. The spectra, then, depend on the radial flow v_r along with M . It has been observed in [17] that for (i) $p_T \gg M$, the radial flow of photons and dileptons are similar, and thus the plateau is achieved. (ii) If the large M pairs originate from early time, when the flow is small, the ratio which includes the space time dynamics will also be close to a static case showing a plateau. (iii) But the plateau disappears when ($p_T \sim M$) or radial flow is large. Here we present the ratio for different lepton pair mass

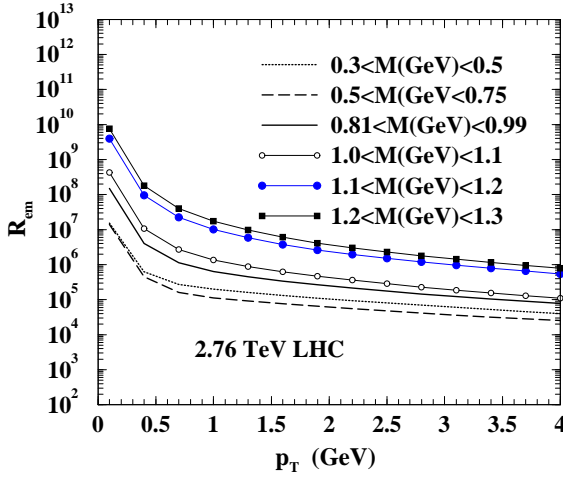


FIG. 8: Ratio of the invariant yield of thermal photons to dileptons at $\sqrt{s_{NN}}=2.76$ TeV LHC energy for different invariant mass windows.

windows for the range of $0.3 < M(\text{GeV}) < 1.3$ at $\sqrt{s_{NN}}=2.76$ TeV.

It may be noted that the ratio of photons to dileptons obtained from pQCD calculation (non-thermal origin) does not show a plateau, which is analysed extensively in [17].

In summary, we say, that the measured direct photon spectra from Au+Au collisions at $\sqrt{s_{NN}}=200$ GeV for 0-5% centrality and from Pb+Pb collisions at $\sqrt{s_{NN}}=2.76$ TeV for 0-40% centrality have been reproduced by ideal relativistic hydrodynamics with an EOS which represents crossover like transition. Initial QGP phase is assumed for both RHIC ($T_i=404$ MeV, $\tau_i=0.2$ fm) and LHC ($T_i=546$ MeV, $\tau_i=0.1$ fm).

It is observed somewhat remarkably that over a wide range of energies going through orders of magnitude, from (even SPS) RHIC to LHC, the thermal photons populate the same p_T window $1.5 \leq p_T(\text{GeV}) \leq 3$. The ratio $\gamma/\mu^+\mu^-$ for the invariant mass window $0.3 < M(\text{GeV}) < 1.3$ and p_T window $1.5 \leq p_T(\text{GeV}) \leq 3$, turns to a plateau indicating the onset of QGP in the heavy ion collision. The formation of thermal window is manifested in the ratio within $1.0 < p_T(\text{GeV}) < 4.0$ at $\sqrt{s_{NN}}=2.76$ TeV LHC energy.

Acknowledgment: JKN thanks P. Mohanty, R. Sahoo, P. Tribedi, N. R. Sahoo, M. Mukherjee, S. Jena, S. Basu, P. Ghosh, T. Nayak and J. Alam for useful discussion. JKN also thanks Swagato Mukherjee of BNL for the discussion on recent lattice data. BS thanks J. Alam, S. Raha, L. McLerran and DAE for Homi Bhabha Chair and the grant associated with it.

-
- [1] I. Arsene *et al.* for BRAHMS collaboration (BRAHMS white paper), Nucl. Phys. A, **757**,1-27 (2005).
 - [2] B. B. Back *et al.* for PHOBOS collaboration (PHOBOS white paper), Nucl. Phys. A **757**, 28-101 (2005).
 - [3] J. Adams *et al.* for STAR collaboration (STAR white paper), Nucl. Phys. A **757**, 102-183 (2005).
 - [4] K. Adcox *et al.* for PHENIX collaboration, PHENIX white paper, Nucl. Phys. A **757**, 184-283 (2005).
 - [5] L. D. McLerran and T. Toimela, Phys. Rev. D **31** 545 (1985).
 - [6] C. Gale and J. I. Kapusta, Nucl. Phys. B **357** 65(1991).
 - [7] H. A. Weldon, Phys. Rev. D **42** 2384 (1990).
 - [8] J. Alam, S. Raha and B. Sinha, Phys. Rep. **273** 243 (1996).
 - [9] Alam J, Sarkar S, Roy P, Hatsuda T and Sinha B, Ann. Phys. **286** 159 (2000).
 - [10] J. Alam, D. K. Srivastava, B. Sinha and D. N. Basu, Phys. Rev. D **48** 1117 (1993).
 - [11] P. Roy, S. Sarkar, J. Alam and B. Sinha, Nucl. Phys. A **653** 277 (1999).
 - [12] J. Alam, S. Sarkar, T. Hatsuda, T. K. Nayak and B. Sinha, Phys. Rev. C **63** 021901(R) (2001).
 - [13] J. Alam, Jajati K. Nayak, P. Roy, A. K. Dutt-Mazumder and B. Sinha, J. Phys. G **34** 871 (2007).
 - [14] P. Mohanty, J. K. Nayak, J. Alam and S. Das, Phys. Rev. C, **82** (2010) 034901.
 - [15] B. Sinha, Phys. Lett. B, **128**,91 (1983); S. Raha and B. Sinha, Phys. Rev. Lett. **58**, 101(1987).
 - [16] D. K. Srivastava and B. Sinha, Phys. Lett. B, **261**,1 (1991).
 - [17] J. K. Nayak, J. Alam, S. Sarkar and B. Sinha, Phys. Rev. C **78** (2008) 034903.
 - [18] J. K. Nayak, J. Alam, S. Sarkar and B. Sinha, J. Phys. G, **35**,104161 (2008).
 - [19] R. Arnaldi *et al* for the NA60 collaboration, Phys. Rev. Lett. **100** 022302 (2008); Eur. Phys. J. C **61**, 711 (2009); S. Damjanovic *et al* for the NA60 Collaboration, J. Phys. G **35**, 104036 (2008).
 - [20] Jajati K. Nayak, J. Alam, T. Hirano, Sourav Sarkar and B. Sinha, Phys. Rev. C **85** 064906 (2012).
 - [21] S. Afanasiev *et al.* for PHENIX collaboration, arXiv:1205.5759 (2012).
 - [22] H. Buesching for PHENIX Collaboration, Nucl. Phys. A **774** 103, (2006)
 - [23] F. Karsch, Nucl. Phys. A **698** 199, (2002).
 - [24] Karel Safarik (for ALICE collaboration), Quark Matter-2012, presentation, to be published.
 - [25] J. K. Nayak, J. Alam, Phys. Rev. C, **80** (2009) 064906.
 - [26] L. E. Gordon and W. Vogelssang, Phys. Rev. D **48**, 3136 (1993).
 - [27] S. Turbide, C. Gale, S. Jeon and G. D. Moore, Phys. Rev. C **72** 014906 (2005); B. G. Zakharov, JETP

- Lett. **80**, 1(2004).
- [28] L. E. Gordon and W. Vogelssang, Phys. Rev. D **50**, 1901 (1994).
 - [29] P. Aurenche *et. al.* Phys. Lett. B **140**, 87 (1984); P. Aurenche *et. al.* Nucl. Phys. B **297**, 661 (1988).
 - [30] J. Kapusta, P. Lichard and D. Seibert, Phys. Rev. D **44** 2774 (1991).
 - [31] R. Baier, H. Nakkagawa, A. Niegawa and K. Redlich, Z. Phys. C **53** 433, (1992).
 - [32] E. Braaten and R. D. Pisarski, Nucl. Phys. B **337** 569 *ibid* **339** 310, (1990).
 - [33] Aurenche P, Gelis F, Zaraket H and Kobes R, Phys. Rev. D **58** 085003 (1998).
 - [34] P. Aurenche, F. Gelis and H. Zaraket, Phys. Rev. D **61**, 116001(2000); P. Aurenche, F. Gelis and H. Zaraket, Phys. Rev. D **62**, 096012(2000).
 - [35] P. Arnold, G. D. Moore and L. G. Yaffe, J. High Energy Phys. **11** 057 (2001); P. Arnold, G. D. Moore and L. G. Yaffe, J. High Energy Phys. **12**, 009 (2001); P. Arnold, G. D. Moore and L. G. Yaffe, J. High Energy Phys. **06**, 30 (2002);
 - [36] T. Renk, Phys. Rev. C **67**, 064901(2003).
 - [37] O. Kaczmarek and F. Zantow, Phys. Rev. D **71**, 114510(2005).
 - [38] J. Alam, P. Roy and S. Sarkar, Phys. Rev. C **71**, 059802 (2005).
 - [39] S. Sarkar, J. Alam, P. Roy, A. K. Dutt-Mazumder, B. Dutta-Roy and B. Sinha, Nucl. Phys. A **634**, 206 (1998).
 - [40] P. Roy, S. Sarkar, J. Alam and B. Sinha, Nucl. Phys. A **653**, 277 (1999).
 - [41] J. Alam, P. Roy and S. Sarkar, Phys. Rev. C **68**, 031901 (R) (2003).
 - [42] S. Turbide, R. Rapp and C. Gale, Phys. Rev. C **69**, 014903(2004).
 - [43] K. L. Haglin, J. Phys. G **30**, L27 (2004)
 - [44] H. von Gersdorff, M. Kataja, L. D. McLerran and P. V. Ruskanen, Phys. Rev. D **34** 794(1986).
 - [45] J. D. Bjorken, Phys. Rev. D **27**, 140 (1983).
 - [46] A. Bazavov *et al.*, Phys. Rev. D, **85** for HotQCD Collaboration, (2012) 054503.
 - [47] M. Cheng *et al.*, Phys. Rev. D, **81** (2010) 054504.
 - [48] S. Gupta, X. Luo, B. Mohanty, H. G. Ritter and N. Xu, Science **332**, 1525(2011).
 - [49] R. C. Hwa and K. Kajantie, Phys. Rev. D, **32** (1985) 1109.
 - [50] M. Asakawa and T. Hatsuda, Phys. Rev. D, **55**(1997)4488.
 - [51] R. Preghenella (for ALICE Collaboration), Acta Physica Pol. B **43** 555 (2011);arXiv:1111.7080.
 - [52] S. Ghosh, S. Mallik and S. Sarkar, Eur. Phys. J. C, **70** ,251 (2010).